

Analysis of Chaos and Regularity in the Open Dicke Model

David Villaseñor¹ and Pablo Barberis-Blostein¹

¹*Instituto de Investigaciones en Matemáticas Aplicadas y en Sistemas,
Universidad Nacional Autónoma de México, C.P. 04510 CDMX, Mexico*

We introduce a criteria to numerically find the complex spectrum of the open Dicke model and present a detailed analysis when dissipation is due to cavity losses. We select two case studies where the classical isolated system shows regularity and where chaos appears. To characterize the open system as regular or chaotic we study regions of the spectrum taking windows over the absolute value of its eigenvalues. Our results agree with the Grobe-Haake-Sommers (GHS) conjecture for Markovian dissipative open quantum systems, finding the expected 2D Poisson distribution for regular regimes, and the distribution of the Ginibre unitary ensemble (GinUE) for the chaotic ones, respectively.

I. INTRODUCTION

The way to characterize the chaotic behavior in isolated quantum systems comes from the classical realm. Classically, the concept of chaos is explained as a strong sensibility to initial conditions. This sensibility is typically measured with the Lyapunov exponent, a rate of divergence between two initially trajectories, which separate between them as time evolves [1]. The extension of the last idea cannot be directly made in the quantum realm, due to the nature of quantum mechanics. Instead, the spectral fluctuations of quantum systems have traditionally been studied, through statistical tests of their eigenvalue spacings [2, 3].

For integrable (regular) quantum systems, the eigenvalue spacings generically follow the Poisson distribution associated with uncorrelated levels, as stated by the Berry-Tabor conjecture [4]. On the other hand, for non-integrable (chaotic) quantum systems with time-reversal symmetry, the spacings follow the Wigner distribution (Wigner surmise) associated with level repulsion. The last was conjectured by Bohigas, Giannoni, and Schmit for quantum systems whose classical limit is chaotic [5], and whose spectral fluctuations are described by the Gaussian orthogonal ensemble (GOE) of the random matrix theory [2, 3, 6]. The last characterization is also applicable for systems without a well-defined classical limit [7–9].

Open quantum systems in the Markovian approximation are studied through a Lindblad master equation, where the dissipation channels take specific forms [10–13]. In this formalism, the dynamics of the system is dictated by an operator called Liouvillian, which is in general non-Hermitian and has complex eigenvalues [14]. The fact that the spectrum of the Liouvillian is complex does not allow a simple generalization of the criteria that characterize the chaotic behavior in open quantum systems, as occurs in isolated systems.

Pioneering studies trying to understand the chaotic nature of open quantum systems were performed in periodically kicked dissipative tops with classical limit [15], where was found that the distribution of the complex-eigenvalue spacings, understood as the Euclidean dis-

tance in the complex plane, follows a 2D (two-dimensional) Poisson distribution when the classical model is regular. The last point is understandable at some extent, since the intuitive extrapolation from isolated regular systems suggests that the spacings must be uncorrelated in the plane. In contrast, the spacing distribution, when the classical model is chaotic, was found to agree with the distribution of the Ginibre unitary ensemble (GinUE) [16], showing a cubic level repulsion [15, 17].

The extrapolation of these results to any dissipative quantum system is nowadays called the Grobe-Haake-Sommers (GHS) conjecture for open quantum systems. It has been shown to be satisfied in other open quantum systems and seems to be universal [17–21].

In this work, we use the Dicke model to characterize the onset of chaos when dissipation is taken into account. The isolated Dicke model represents the simplest interacting radiation-matter system [22–24]. It was introduced originally to explain superradiance [22], and in recent years it has been used in a broad variety of theoretical studies, including quantum phase transitions [25–28], classical and quantum chaos [29–36], quantum scarring [36–41], quantum localization in phase space [42–44], non-equilibrium quantum dynamics [24, 45–49], evolution of out-of-time-ordered correlators (OTOCs) [50–53], connections between chaos, entanglement [35, 36, 54], and thermalization [53, 55, 56], among others.

The Dicke model can be experimentally realized with setups as diverse as superconducting circuits [57], cavity assisted Raman transitions [58, 59], trapped ions [60, 61], and others. On the other hand, this model has a well-defined classical limit with two-degrees of freedom [29, 34]; which, depending on the parameters and energy regions, can show regular or chaotic motion.

Some versions of the open Dicke model with cavity dissipation or collective atomic dissipation have been already studied. The theoretical aspects investigated in these works range from superradiance and quantum phase transitions [62–67], to classical and quantum chaos [68–70]. Some studies have focused in a particular version of the model, as the two-photon open Dicke model [71, 72]. Moreover, experimental realizations of the open Dicke model with optical cavities are shown in

Refs. [73, 74].

The main goal in this work is to propose a method to study the complex spectrum of the open Dicke model and characterize the onset of chaos in the system. Due to the infinite-dimensional Liouville space of the open Dicke model, a truncation must be made, which introduces error in the solutions, when the system is solved numerically. In this regard, we propose a convergence criterion for eigenstates and eigenvalues of the system, to discriminate in a consistent way those that are not real solutions of the system. Achieving the last condition, we apply the standard methodology of open quantum systems to reveal the appearance of chaotic behavior in the open Dicke model. Despite there are some studies focused in the classical limit of the open Dicke model [68, 72], in this work we restrict ourselves to the quantum treatment of chaos.

The article is organized as follows. In Sec. II, we introduce the isolated Dicke model, represented by the Dicke Hamiltonian, and its more important features. Next, we introduce the open Dicke model, represented by the Dicke Liouvillian, which defines the evolution of the system density matrix through a Lindblad master equation in the Markovian approximation. We mention the most important features of the open system also, as the dissipative phase transition. In Sec. III, we propose a convergence criterion for the eigenstates and eigenvalues of the Dicke Liouvillian, which is implemented via exact diagonalization. In Sec. IV, we show the standard procedures to perform the spectral analysis in open quantum systems, as well as a brief review of the spectral analysis in isolated quantum systems. The main results of the article concerning chaos and regularity in the open Dicke model are shown in Sec. V. Finally, our conclusions are summarized and presented in Sec. VI.

II. OPEN DICKE MODEL

The Dicke model, which describes the interaction between a set of \mathcal{N} two-level atoms and a single-mode electromagnetic field without dissipation channels (isolated system), is represented by the Hamiltonian (setting $\hbar = 1$) [22]

$$\hat{H}_D = \omega \hat{a}^\dagger \hat{a} + \omega_0 \hat{J}_z + \frac{\gamma}{\sqrt{\mathcal{N}}} (\hat{a}^\dagger + \hat{a})(\hat{J}_+ + \hat{J}_-), \quad (1)$$

where \hat{a}^\dagger (\hat{a}) is the bosonic creation (annihilation) operator of the field mode. The set of operators $\{\hat{a}^\dagger, \hat{a}, \hat{1}\}$ satisfy the (Heisenberg-Weyl) $H(1)$ algebra. Moreover, \hat{J}_+ (\hat{J}_-) is the raising (lowering) collective pseudo-spin operator, defined as $\hat{J}_\pm = \hat{J}_x \pm i\hat{J}_y$, where $\hat{J}_{x,y,z} = (1/2) \sum_{k=1}^{\mathcal{N}} \hat{\sigma}_{x,y,z}^k$ are the collective pseudo-spin operators and $\hat{\sigma}_{x,y,z}$ are the Pauli matrices. The set of operators $\{\hat{J}^+, \hat{J}_-, \hat{J}_z\}$ satisfy the $SU(2)$ algebra in the same way as the Pauli matrices.

The Dicke Hamiltonian can be studied in invariant subspaces specified by the eigenvalues $j(j+1)$ of the squared

total pseudo-spin operator $\hat{\mathbf{J}}^2 = \hat{J}_x^2 + \hat{J}_y^2 + \hat{J}_z^2$. We use the totally symmetric subspace, which is defined by the maximum pseudo-spin value $j = \mathcal{N}/2$ and includes the ground state. Furthermore, the Dicke Hamiltonian possesses a parity symmetry, $[\hat{H}_D, \hat{\Pi}] = 0$, where the parity operator $\hat{\Pi} = \exp[i\pi(\hat{a}^\dagger \hat{a} + \hat{J}_z + j\hat{1})]$ identifies states in two sectors of well-defined parity.

The main parameters of the Dicke Hamiltonian are the radiation frequency of the single-mode electromagnetic field, ω , the atomic transition frequency from the ground state to the first excited state, ω_0 , and the coupling strength, γ , which modulates the atom-field interaction within the system and reaches the critical value $\gamma_c = \sqrt{\omega\omega_0}/2$. At this value, the system develops a quantum phase transition going from a normal ($\gamma < \gamma_c$) to a superradiant ($\gamma > \gamma_c$) phase [25, 75–77]. Classically, the Dicke model displays regular or chaotic behavior depending on the latter Hamiltonian parameters (ω, ω_0, γ) and the excitation energies [34].

When dissipation due to cavity losses is included in the system, the open Dicke model can be studied with the standard treatment in the Markovian approximation for open quantum systems, through a Lindblad master equation of the form (setting $\hbar = 1$) [10–12]

$$\frac{d\hat{\rho}}{dt} = \hat{\mathcal{L}}_D \hat{\rho} = -i[\hat{H}_D, \hat{\rho}] + \kappa(2\hat{a}\hat{\rho}\hat{a}^\dagger - \{\hat{a}^\dagger \hat{a}, \hat{\rho}\}), \quad (2)$$

where $\hat{\rho}$ defines the state of the system in the Liouville space (density matrix of the system in the Hilbert space of the isolated system), κ is the cavity decay coupling, and $\hat{\mathcal{L}}_D$ is the Liouville superoperator or Dicke Liouvillian, which acts over states in the Liouville space (operators in the Hilbert space of the isolated system). The study presented here could be extended to more general dissipation channels, as those including collective atomic decay or considering temperature effects [10–12, 24, 78]. Moreover, the Dicke Liouvillian inherits a weak-parity symmetry of the Hamiltonian [79–81], since $[\hat{\mathcal{L}}_D, \hat{\mathcal{P}}] = 0$, where the parity superoperator $\hat{\mathcal{P}}\hat{\rho} = \hat{\Pi}\hat{\rho}\hat{\Pi}^\dagger$ identifies states with well-defined parity in the Liouville space.

On the other hand, when cavity dissipation is considered in the open Dicke model, a quantum dissipative phase transition takes place at the critical coupling strength [24, 62, 78]

$$\gamma_c^{\text{os}} = \frac{\sqrt{\omega\omega_0}}{2} \sqrt{1 + \frac{\kappa^2}{\omega^2}}, \quad (3)$$

defining, analogously to the isolated system, two phases in the open system, a normal ($\gamma < \gamma_c^{\text{os}}$) and a superradiant ($\gamma > \gamma_c^{\text{os}}$) dissipative phase, respectively.

In this work, we use dimensionless Hamiltonian parameters scaled to the cavity decay coupling κ , $(\tilde{\omega}, \tilde{\omega}_0, \tilde{\gamma}) = (\omega/\kappa, \omega_0/\kappa, \gamma/\kappa)$. For convenience, we remove the tilde from the last scaled parameters. We choose the resonant frequency case $\omega = \omega_0 = 1$, such that, the critical coupling strength value of the isolated and open system is $\gamma_c = 0.5$ and $\gamma_c^{\text{os}} = 1/\sqrt{2} \approx 0.707$, respectively. With

the selected parameters, we can consider two case studies, one with a coupling strength in the normal phase ($\gamma = 0.2$), and another one in the superradiant phase ($\gamma = 1$) of the open system. For these values, the classical isolated system shows regular and chaotic motion, respectively [34]. Moreover, in order to perform the spectral analysis we select the sector of eigenstates (eigenvalues) with positive parity in the Liouville space (see App. A for an explanation of the Dicke Liouvillian with well-defined parity). To begin with a systematic analysis, we choose the smallest system size $j = 1$ ($\mathcal{N} = 2$ atoms).

III. CONVERGENCE OF EIGENVALUES AND EIGENSTATES OF THE OPEN DICKE MODEL

The isolated Dicke model has an infinite-dimensional Hilbert space composed by a finite atomic subspace with dimension $2j + 1$, and an infinite bosonic subspace. To solve this model numerically, a truncation of the Hilbert space by a finite value of the photon number n_{\max} is needed, generating this way a finite Hilbert space with dimension $\mathcal{D}_H = (2j + 1)(n_{\max} + 1)$. In the Liouville representation, the new space (Liouville space) is also infinite, and a truncation of the same is needed to solve it numerically. A finite Liouville space can be obtained through the truncated Hilbert space, where the Liouville basis is composed by all the projectors of the basis states of the truncated Hilbert space. Thus, the Liouville space dimension is the square of the Hilbert space dimension $\mathcal{D}_L = \mathcal{D}_H^2$. Nevertheless, the eigenstates and eigenvalues of the truncated matrix do not necessarily are eigenstates and eigenvalues of the full infinite matrix. In this section we introduce a convergence criterion to find eigenstates (eigenvalues) that are numerically close to the eigenstates (eigenvalues) of the full matrix.

A. Convergence of Eigenvalues

A usual way to define convergence of eigenvalues in infinite-dimensional spaces is comparing the change of the eigenvalues ε_k for two truncation values, n_{\max} and $n_{\max} + 1$,

$$\Delta\varepsilon_k = |\varepsilon_k^{n_{\max}+1} - \varepsilon_k^{n_{\max}}| \leq \epsilon, \quad (4)$$

where ϵ is a tolerance value. Thus, the eigenvalue ε_k is rejected when the change $\Delta\varepsilon_k$ exceeds the threshold ϵ .

This method has been successfully tested in the eigenvalues of the Dicke Hamiltonian [82], but the implementation becomes computing demanding when the truncation size of the Hamiltonian matrix increases, since two diagonalizations are needed. For this reason, an alternative convergence criterion based on the eigenstates of the truncated Hamiltonian matrix was proposed, showing an equivalence with the eigenvalue convergence criterion and using only one diagonalization of the system [83].

When extending the eigenvalue convergence criterion to the Dicke Liouvillian, we found it is not applicable. We suspect that the complex spectrum of the Dicke Liouvillian is a continuous spectrum, since each diagonalization of the system with a fixed truncation value n_{\max} generates a new set of eigenvalues, which were not present in the previous diagonalization with a smaller truncation value. It is well known that for complex non-Hermitian matrices, always there is a set of eigenvalues missed in the complex plane [84].

B. Convergence of Eigenstates

Since the eigenvalue convergence criterion is not applicable to the Dicke Liouvillian, we propose in this work an extension of the eigenstate convergence criterion of the Dicke Hamiltonian for the Dicke Liouvillian. A detailed description of this criterion for the Dicke Hamiltonian and its validity are presented in Ref. [83]. The eigenstates of Dicke Hamiltonian can be expanded in an arbitrary basis. Typically the Fock basis $|f\rangle = |n; j, m_z\rangle$ (with $n = 0, 1, \dots, n_{\max}$ and $m_z = -j, -j + 1, \dots, j - 1, j$) is used to diagonalize the Hamiltonian and the eigenstates of the system, $\hat{H}_D|E_k\rangle = E_k|E_k\rangle$, have the following representation

$$|E_k\rangle = \sum_{f=1}^{\mathcal{D}_H} c_f^k |f\rangle = \sum_{n=0}^{n_{\max}} \sum_{m_z=-j}^j c_{n,m_z}^k |n; j, m_z\rangle, \quad (5)$$

where $c_f^k = \langle f|E_k\rangle$ or $c_{n,m_z}^k = \langle n; j, m_z|E_k\rangle$, and the eigenstates are arranged in increasing order of their real eigenvalues $E_k \leq E_{k+1}$, $E_k \in \mathbb{R}$.

The probability to have n photons in the eigenstate $|E_k\rangle$ is given by

$$p_n^k = \sum_{m_z=-j}^j |\langle n; j, m_z|E_k\rangle|^2 = \sum_{m_z=-j}^j |c_{n,m_z}^k|^2, \quad (6)$$

and when this probability is evaluated for all the values $n = 0, 1, \dots, n_{\max}$, it can be interpreted as a projection of the eigenstate wave function over the Fock basis. In this way, an eigenstate convergence criterion is proposed as to have zero probability for the maximum number of photons n_{\max} , or equivalently, to have the eigenstate wave function contained in the truncated Hilbert space, that is, all coefficients contributing to the wave function must be contained inside the truncated Hilbert space

$$p_{n_{\max}}^k = \sum_{m_z=-j}^j |c_{n_{\max},m_z}^k|^2 \leq \delta, \quad (7)$$

where δ is a tolerance value.

The last convergence criterion can be extended for the eigenstates of the Dicke Liouvillian. By considering the Liouville basis as the projectors of the Fock basis $|f', f\rangle = |f'\rangle\langle f| = |n'; j, m'_z\rangle\langle n; j, m_z|$ (with $n', n =$

$0, 1, \dots, n_{\max}$ and $m'_z, m_z = -j, -j+1, \dots, j-1, j$), we can diagonalize the Liouvillian and the eigenstates of the open system, $\hat{\mathcal{L}}_D|\lambda_k\rangle = \lambda_k|\lambda_k\rangle$, take the form

$$\begin{aligned} |\lambda_k\rangle &= \sum_{f', f=1}^{\mathcal{D}_H} c_{f', f}^k |f', f\rangle = \sum_{f'=1}^{\mathcal{D}_H} \sum_{f=1}^{\mathcal{D}_H} c_{f', f}^k |f'\rangle \langle f| \quad (8) \\ &= \sum_{n'=0}^{n_{\max}} \sum_{m'_z, m_z=-j}^j c_{n', m'_z, n, m_z}^k |n'; j, m'_z\rangle \langle n; j, m_z|, \end{aligned}$$

where $c_{f', f}^k = \langle\langle f', f | \lambda_k \rangle\rangle$, and the eigenstates are arranged in increasing order of their complex-eigenvalue absolute values $|\lambda_k| \leq |\lambda_{k+1}|$, $\lambda_k \in \mathbb{C}$.

Analogously to the isolated system, we can define an extension of Eq. (6) for the eigenstate $|\lambda_k\rangle$ of the open system, such that, we have two weight distributions

$$P_{1, n'}^k = \sum_{n=0}^{n_{\max}} \sum_{m'_z, m_z=-j}^j |c_{n', m'_z, n, m_z}^k|^2, \quad (9)$$

$$P_{2, n}^k = \sum_{n'=0}^{n_{\max}} \sum_{m'_z, m_z=-j}^j |c_{n', m'_z, n, m_z}^k|^2, \quad (10)$$

which can be interpreted as projections of the eigenstate wave function over the Liouville basis for all the values $n', n = 0, 1, \dots, n_{\max}$.

Thus, the extension of the eigenstate convergence criterion for the Dicke Liouvillian is proposed as to have zero contribution of the weight distribution for the maximum number of photons n_{\max} , or to have the eigenstate wave function contained in the truncated Liouville space for both projections

$$P_{1, n_{\max}}^k = \sum_{n=0}^{n_{\max}} \sum_{m'_z, m_z=-j}^j |c_{n_{\max}, m'_z, n, m_z}^k|^2 \leq \Delta, \quad (11)$$

$$P_{2, n_{\max}}^k = \sum_{n'=0}^{n_{\max}} \sum_{m'_z, m_z=-j}^j |c_{n', m'_z, n_{\max}, m_z}^k|^2 \leq \Delta, \quad (12)$$

where Δ is a tolerance value.

C. Convergence of Eigenstates vs. Eigenvalues

In order to show that the convergence criterion proposed in the last section for eigenstates of the Dicke Liouvillian can be used to select their corresponding well-converged eigenvalues, we present in this section numerical results implementing it.

We select a set of truncation values of the Liouville space $n_{\max} = 10, 20, 30, 40, 50, 60$ and diagonalize the Dicke Liouvillian for the parameters presented previously $\omega = \omega_0 = j = \kappa = 1$. We perform this procedure for two cases $\gamma = 0.2$ and $\gamma = 1$ to ensure we are diagonalizing the system in the normal ($\gamma < \gamma_c^{\text{os}}$) and superradiant ($\gamma > \gamma_c^{\text{os}}$) dissipative phase, respectively.

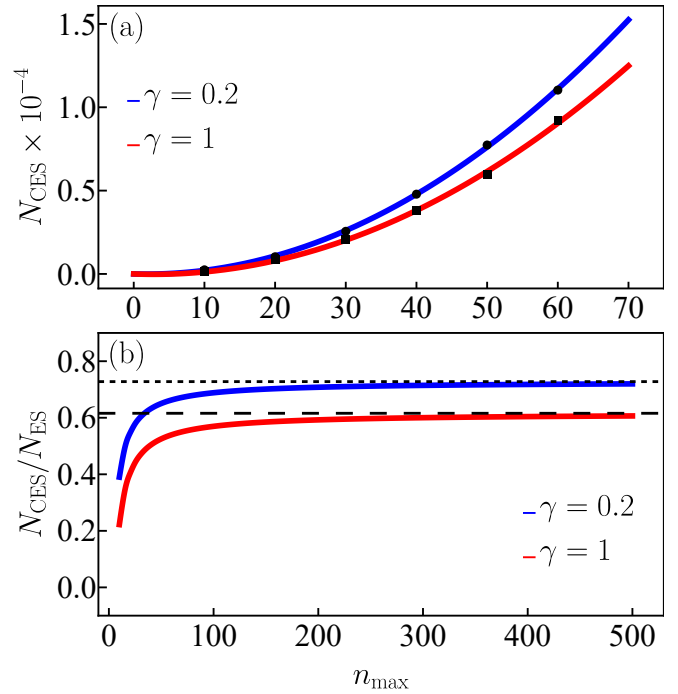


FIG. 1. Panel (a): Number of converged eigenstates N_{CES} with positive parity of the Dicke Liouvillian for two coupling strength values $\gamma = 0.2$ (black dots) and $\gamma = 1$ (black squares), which were computed numerically for the truncation values $n_{\max} = 10, 20, 30, 40, 50, 60$. The solid blue (red) curve depicts an analytical fit of the black dots (squares). Panel (b): Ratio of the number of converged eigenstates N_{CES} to the total number of eigenstates N_{ES} for the same coupling strength values $\gamma = 0.2$ (blue curve) and $\gamma = 1$ (red curve). The black dotted (dashed) horizontal line represents the asymptotic value of the last ratio in the limit $n_{\max} \rightarrow \infty$ (see Eq. (15)). The Liouvillian parameters in both panels are $\omega = \omega_0 = j = \kappa = 1$ and the tolerance value was chosen as $\Delta = 10^{-3}$.

We use the Liouville basis with positive parity ($P = +1$) to perform the convergence analysis and at the same time, to perform the spectral analysis in Sec V. See App. A for a complete description on how to diagonalize the Dicke Liouvillian using the Liouville basis and how to select the basis with well-defined parity. For the well-defined parity Liouville basis, the dimension of the Liouville space $\mathcal{D}_{L, P}$ (which defines the number of eigenstates N_{ES}) is given by

$$\begin{aligned} N_{\text{ES}} &= \mathcal{D}_{L, P=\pm 1} \quad (13) \\ &= \begin{cases} \mathcal{D}_H^2/2 & \text{if } (-1)^{n_{\max}} = -1 \\ (\mathcal{D}_H^2 \pm 1)/2 & \text{if } (-1)^{n_{\max}} = 1 \end{cases}, \end{aligned}$$

where $\mathcal{D}_H = (2j + 1)(n_{\max} + 1)$ is the dimension of the Hilbert space of the isolated system.

In Fig. 1 (a) we show the number of well-converged eigenstates N_{CES} selected under the eigenstate convergence criterion (see Eqs. (11) and (12)) with a tolerance value $\Delta = 10^{-3}$, for all the truncation values

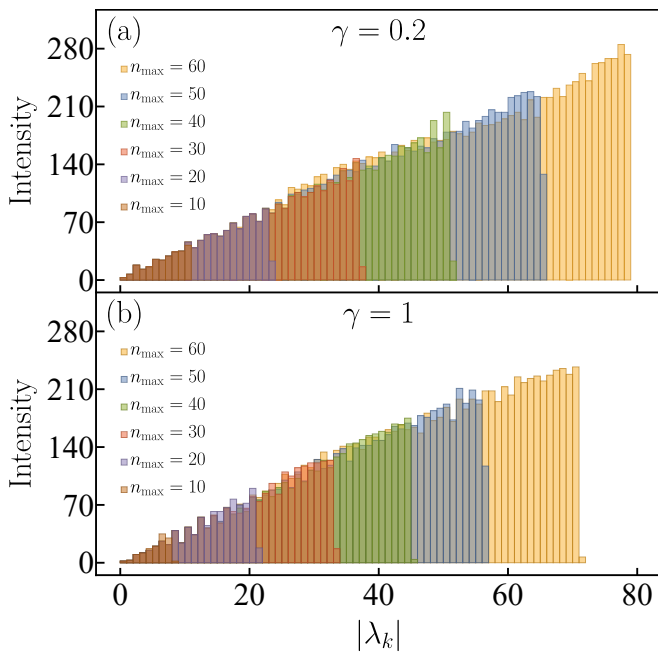


FIG. 2. Panel (a): Histogram of the absolute value of the converged eigenvalues $|\lambda_k|$ with positive parity of the Dicke Liouvillian for the coupling strength $\gamma = 0.2$, which were computed numerically for the truncation values $n_{\max} = 10, 20, 30, 40, 50, 60$. Panel (b): The same as panel (a) for the coupling strength $\gamma = 1$. The Liouvillian parameters in both panels are $\omega = \omega_0 = j = \kappa = 1$ and the tolerance value was chosen as $\Delta = 10^{-3}$.

$n_{\max} = 10, 20, 30, 40, 50, 60$. By fitting the numerical results, we find a quadratic behavior for the number of converged eigenstates

$$N_{\text{CES}} = A_1 n_{\max} + A_2 n_{\max}^2, \quad (14)$$

where $A_1 = -11.49, -15.60$ and $A_2 = 3.28, 2.77$ identify the fitting values for each coupling strength $\gamma = 0.2, 1$.

Using the last analytical expressions, we can find their asymptotic value in the limit $n_{\max} \rightarrow \infty$ for the ratio of converged eigenstates to the total number of eigenstates obtained in each implementation

$$\lim_{n_{\max} \rightarrow \infty} \frac{N_{\text{CES}}}{N_{\text{ES}}} = \frac{2A_2}{(2j+1)^2}. \quad (15)$$

For the parameters $A_2 = 3.28, 2.77$ we find the asymptotic values 0.729 and 0.616, respectively. In Fig. 1 (b) we show the ratio $N_{\text{CES}}/N_{\text{ES}}$ as a function of the truncation value n_{\max} , with their corresponding asymptotic value for the cases $\gamma = 0.2, 1$. We see in this figure, that the fraction of converged eigenstates is bounded for both cases, tending asymptotically to a constant value in the limit $n_{\max} \rightarrow \infty$.

Now, we consider an eigenvalue λ_k well converged, when its corresponding eigenstate $|\lambda_k\rangle\rangle$ fulfills the last criterion. Thus, we take the converged eigenvalues for

the set $n_{\max} = 10, 20, 30, 40, 50, 60$ and present the histogram of their absolute value $|\lambda_k|$ in Fig. 2 for both cases $\gamma = 0.2, 1$. These histograms can be interpreted as a density of states for the absolute value $|\lambda_k|$. In both cases $\gamma = 0.2, 1$, we find that increasing the truncation value n_{\max} preserves the behavior of the density of states. Furthermore, we see a number of converged eigenvalues higher for the low coupling strength $\gamma = 0.2$ than for the high one $\gamma = 1$. The last finding is intuitive extrapolating from the isolated system. In general, there are less converged eigenstates (eigenvalues) when the coupling strength is high in the system, since the eigenstate wave functions are more spread in the diagonalization basis and the convergence criterion is more difficult to be fulfilled [82, 83].

It is important to highlight that, when the complete sets of eigenvalues (converged and not converged) are taken into account, the overall statistical behavior is the same for all the truncation values of the Liouville space. That is, our method only discriminates eigenvalues, whose eigenstates do not fulfill the proposed eigenstate convergence criterion (see Eqs. (11) and (12)), but the overall statistical behavior of the eigenvalues remains the same. The last feature allows us to work with a reasonable convergence criterion for eigenstates (eigenvalues) of the Dicke Liouvillian.

To explain deeper our convergence criterion, we focus on a single truncation value, the higher one $n_{\max} = 60$, for which we have obtained $N_{\text{CES}} = 11030, 9165$ converged eigenstates (eigenvalues) for the cases $\gamma = 0.2, 1$ with a tolerance value $\Delta = 10^{-3}$. In Fig. 3 we show the case $\gamma = 0.2$, where the complex spectrum ordered by the eigenvalue absolute value $|\lambda_k|$ is presented in panel (a1), where the black dots represent the complete set of eigenvalues, while the blue dots represent the converged ones.

Panels (a2)-(a3) in Fig. 3 show the convergence criterion computed for all eigenstates $|\lambda_k\rangle\rangle$ (see Eqs. (11) and (12)). In the same way, the black dots represent the criterion computed for all the set of eigenstates, while the blue dots for the converged ones. In these panels a fraction of eigenstates for which the criterion is apparently fulfilled can be seen beyond $k = 15000$ and even for the region $k > 10000$, where the lack of convergence arises. Nevertheless, to avoid ambiguities by selecting them, and recalling that they are ordered with the increasing eigenvalue absolute value $|\lambda_k|$, we select them until the first eigenstate does not fulfill the criterion, discarding the remaining ones.

In Fig. 3 (b1) we show the spectrum in the complex plane, where it is more obvious the region of the well-converged spectrum as a stain. In this panel and panels (a1)-(a3), a 3D diamond representing a particular eigenvalue (eigenstate) with label $k = 6000$ is shown. In panels (b2)-(b3) we show its wave function projections over the Liouville basis (see Eqs. (9) and (10)), where we can see, as we have argued previously, that the wave function is contained in the truncated Liouville space for both pro-

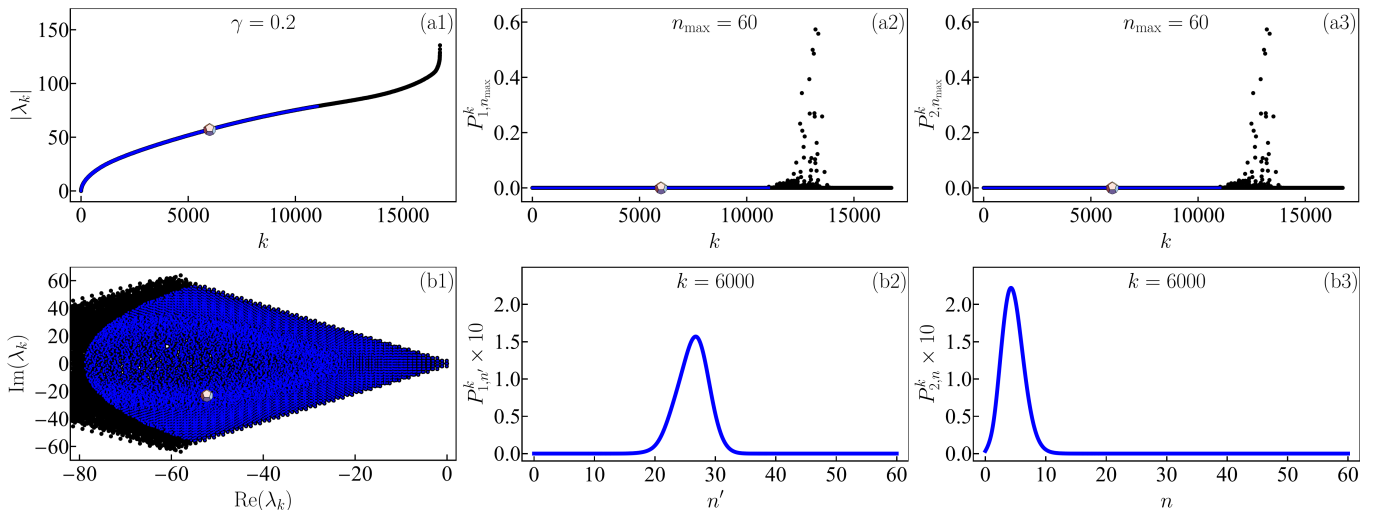


FIG. 3. Panel (a1): Absolute value of the eigenvalues $|\lambda_k|$ (black dots) with positive parity of the Dicke Liouvillian for the coupling strength $\gamma = 0.2$, which were computed numerically for the truncation value $n_{\max} = 60$. The blue dots represent the well-converged eigenvalues selected under the eigenstate convergence criterion, and the diamond selects the eigenvalue with label $k = 6000$, λ_{6000} . Panels (a2)-(a3): Convergence criterion for the eigenstates $|\lambda_k\rangle$ with positive parity of the Dicke Liouvillian (see Eqs. (11) and (12)). Panel (b1): Complex spectrum of the Dicke Liouvillian. Panels (b1)-(b2): Wave function projections of the selected eigenstate $|\lambda_{6000}\rangle$ (see Eqs. (9) and (10)). The Liouvillian parameters in all panels are $\omega = \omega_0 = j = \kappa = 1$ and the tolerance value was chosen as $\Delta = 10^{-3}$.

jections, ensuring this way its convergence.

We repeat the last analysis for the case $\gamma = 1$, showing the results in Fig. 4. For this case, we see the same overall behaviour, with slightly differences. For the high coupling strength case we find less converged eigenvalues as for the low one. The last feature is well understood by analyzing panel (b2) in Fig. 4. For this projection, the eigenstate wave function looks more spread over the Liouville basis. This is feature which show typically chaotic eigenstates, they are expanded in all accessible Hilbert (Liouville) space, resembling a random state [85]. Panel (b3) in Fig. 4 shows the projection of the eigenstate wave function not spread at all over the Liouville basis, which shows that the eigenstate wave function has a very complex structure in Liouville space, and these projections are useful tools to understand it.

IV. SPECTRAL ANALYSIS AND QUANTUM CHAOS IN OPEN QUANTUM SYSTEMS

The way to perform the spectral analysis for open quantum systems with complex spectra was first outlined in Ref. [15]. The studies were latter extended to other open quantum systems, which suggest that the behavior regarding regularity and chaos in dissipative systems is universal [18]. We follow the procedure exposed in these references in the present work.

A. Eigenvalue Spacing Distributions for Regular and Chaotic Complex Spectra

In isolated quantum systems, where the Hamiltonians are Hermitian with real eigenvalues, $\varepsilon_k \in \mathbb{R}$, the notion of spacing comes from the fact that we can order a finite set of eigenvalues in increasing order, $\varepsilon_k \leq \varepsilon_{k+1}$, where the spacing is defined as the separation between an eigenvalue ε_k and its nearest neighbor ε_{k+1} , $s_k = \varepsilon_{k+1} - \varepsilon_k$. Performing an unfolding procedure of the spectrum, we can study its spectral fluctuations using the nearest-neighbor spacing distribution, which follow typically the Poisson distribution, $P_P(s) = \exp(-s)$, for integrable (regular) systems and the Wigner-Dyson surmise, $P_{WD}(s) = (\pi/2)s \exp(-\pi s^2/4)$, for the non-integrable (chaotic) ones [3, 5].

For open quantum systems, the Liouvillians are non-Hermitian and the eigenvalues are complex, $\varphi_k \in \mathbb{C}$, such that, the standard treatment to analyze spectral fluctuations is not applicable anymore. As the eigenvalues are complex numbers, they can be plotted in the complex plane (see Fig. 3 (b1) and Fig. 4 (b1) for the complex eigenvalues of the Dicke Liouvillian). For these systems, the spacing is understood as the minimal Euclidean distance in the complex plane for an eigenvalue φ_k and its nearest neighbor φ_k^{1N} , $s_k = |\varphi_k - \varphi_k^{1N}|$. After performing an unfolding procedure for complex spectra (see App. B for a complete explanation of this technique), we can study analogously to the isolated systems, the spectral fluctuations in the open systems.

Typically, the nearest-neighbor spacing distribution for integrable (regular) open quantum systems follows a 2D

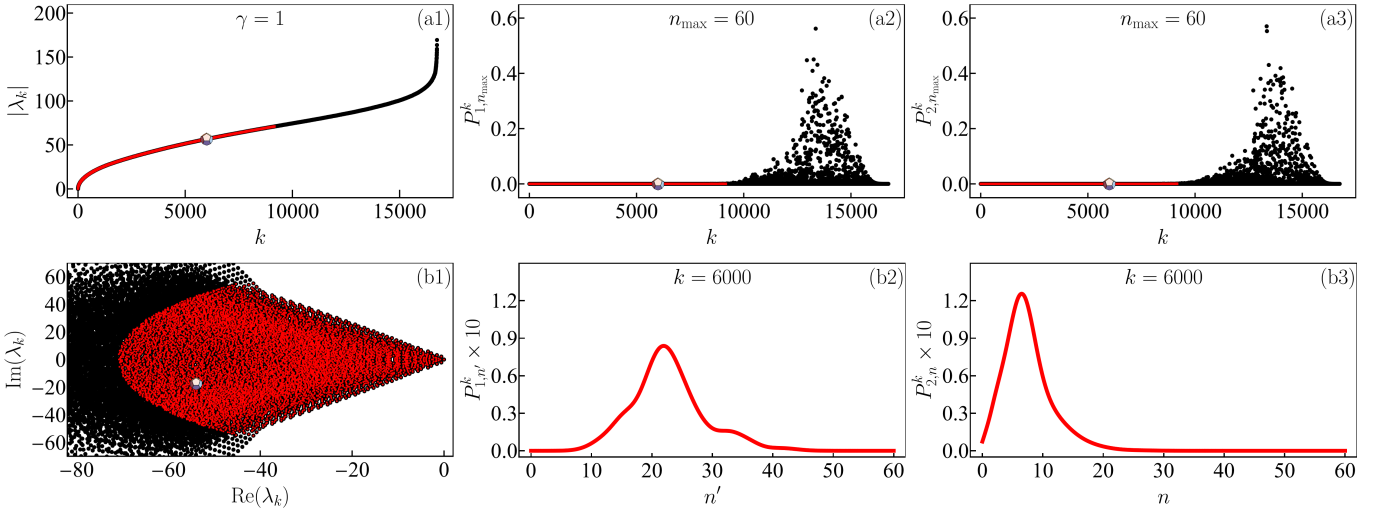


FIG. 4. The same as Fig. 3 for the coupling strength $\gamma = 1$.

Poisson distribution [2, 15, 18], which is given by

$$P_{2\text{DP}}(s) = \frac{\pi}{2} s e^{-\pi s^2/4}. \quad (16)$$

Note that this distribution is functionally the same as the Wigner-Dyson surmise, which characterizes the chaotic cases in isolated quantum systems.

On the other hand, for non-integrable (chaotic) open quantum systems, the nearest-neighbor spacing distribution follows the distribution of the Ginibre unitary ensemble (GinUE) [2, 15, 16, 18, 20], given by

$$P_{\text{GinUE}}(s) = \prod_{k=1}^{\infty} \frac{\Gamma(1+k, s^2)}{k!} \times \sum_{k'=1}^{\infty} \frac{2s^{2k'+1} e^{-s^2}}{\Gamma(1+k', s^2)}, \quad (17)$$

where $\Gamma(k, z) = \int_0^{\infty} dt t^{k-1} e^{-t}$ is the incomplete Gamma function, $\int_0^{\infty} ds P_{\text{GinUE}}(s) = 1$, and $\bar{s} = \int_0^{\infty} ds s P_{\text{GinUE}}(s) \approx 1.1429$. In order to compare this distribution with numerical values, a scaling must be made to ensure its first moment is unity

$$\tilde{P}_{\text{GinUE}}(s) = \bar{s} P_{\text{GinUE}}(\bar{s}s), \quad (18)$$

with $\int_0^{\infty} ds \tilde{P}_{\text{GinUE}}(s) = 1$ and $\int_0^{\infty} ds s \tilde{P}_{\text{GinUE}}(s) = 1$.

In the limit $s \rightarrow 0$, both distributions tend to the power law

$$P_{\beta}(s) \propto s^{\beta}, \quad (19)$$

where the power $\beta = 1, 3$ identifies the degree of level repulsion, linear (regular) for integrable cases and cubic for non-integrable (chaotic) ones, which seems to be universal in open quantum systems [2, 15, 17].

In order to corroborate that a data set comes from a given distribution, the well-known Anderson-Darling test can be implemented for the spacings $s_k = |\varphi_k - \varphi_k^{1N}|$, by

computing the parameter [86]

$$A^2 = -N - \sum_{k=1}^N \frac{2k-1}{N} (\ln[F_X(s_k)] + \ln[1 - F_X(s_{N+1-k})]), \quad (20)$$

where the spacings are arranged in increasing order $s_k \leq s_{k+1}$, and $F_X(s) = \int_0^s ds' P_X(s')$ is the cumulative distribution function of the probability distribution $P_X(s)$ with $X=2\text{DP}, \text{GinUE}$. When the Anderson-Darling parameter is greater than a threshold, $A^2 > 2.5$, we can conclude with 95% of confidence that the data set does not come from the given probability distribution.

B. Ratio of Consecutive Eigenvalue Spacings for Complex Spectra

The ratio of consecutive eigenvalue spacings was introduced to study spectral fluctuations in isolated systems with real eigenvalues [87, 88]. The advantage of this test is that the spectra can be studied without implementing unfolding procedures, which can be ambiguous in some cases. The last test can be extended to open systems with complex eigenvalues. The procedure is detailed in Ref. [89], where the complex ratio takes the form

$$Z_k = r_k e^{i\theta_k} = \frac{\varphi_k^{1N} - \varphi_k}{\varphi_k^{2N} - \varphi_k}, \quad (21)$$

where φ_k^{1N} and φ_k^{2N} are the first and second nearest neighbor of an eigenvalue φ_k , respectively.

The generic results from isolated quantum systems, where the eigenvalues of integrable quantum systems are uncorrelated (Poisson distribution) and those of non-integrable ones show level repulsion (Wigner-Dyson surmise), can be extended to open quantum systems. In

open quantum systems, the sets of eigenvalues of integrable systems (2D Poisson distribution) are uncorrelated in the complex plane showing a flat (delocalized) distribution. On the other hand, the sets of eigenvalues of non-integrable systems (GinUE distribution) shows level repulsion, which manifests itself with a suppression of the distribution at the origin and small angles [89].

The expectation values of $r_k = |Z_k|$ and $\cos(\theta_k) = \text{Re}(Z_k)/r_k$ can be computed using the marginal distributions from each distribution 2DP and GinUE. The following results are obtained $\langle r_k \rangle_X = 2/3, 0.74$ and $-\langle \cos(\theta_k) \rangle_X = 0, 0.24$ with $X=2DP, \text{GinUE}$; which can be used as a benchmark to validate numerical results.

V. CHAOS AND REGULARITY IN THE OPEN DICKE MODEL

In this section we show numerical results characterizing the complex spectrum of the Dicke Liouvillian as chaotic or regular. To achieve this goal we choose the spectrum computed with the highest truncation value $n_{\text{max}} = 60$, which was already presented in Sec. III C. For this truncation value ($n_{\text{max}} = 60$) we get $N_{\text{CES}} = 11030, 9165$ converged eigenstates (eigenvalues) for the coupling strengths $\gamma = 0.2, 1$, with a tolerance value $\Delta = 10^{-3}$ (see Fig. 3 (a1) and Fig. 4 (a1), respectively).

As a first case study, we present the case $\gamma = 1$, whose isolated classical system shows chaotic behavior [34]. The way to study the complex spectrum of the Dicke Liouvillian must be dealt with care, since there is a well-studied characterization of the real spectrum of the Dicke Hamiltonian for coupling strengths in the superradiant phase ($\gamma > \gamma_c$), where at low energies the spectral fluctuations are regular (Poisson distribution), while for high energies the spectral fluctuations become chaotic (Wigner-Dyson surmise) [30, 31]. That is, the real spectrum of the isolated system transits from regularity at low energies to chaos at high energies. The last can be understood also from the classical Dicke Hamiltonian, where at low energies near the ground state energy, the system can be approximated as a harmonic oscillator obtaining regular motion; while at high energies, the system develops chaotic motion [34].

Based on this background, it is intuitive that the open system could inherit some properties of the isolated system; that is, the complex spectrum of the Dicke Liouvillian must be studied by regions, where the chaotic or regular behavior can arise, as occurs with the real spectrum of the Dicke Hamiltonian. The way to detect these regions is not obvious, since we do not have studied yet a classical limit of the open Dicke model, which could serve as a benchmark.

Next, we propose to study the complex spectrum of the Dicke Liouvillian taking regions organized by the increasing absolute value of its eigenvalues, as shown in Fig. 2 (b). As was argued previously, these histograms can be interpreted as a density of states for the eigenvalue

absolute value $|\lambda_k|$. We take moving windows of 500 consecutive eigenvalues and apply the Anderson-Darling test to the eigenvalues contained in these windows, by computing the Anderson-Darling parameter (see Eq. (20)). The moving windows run from the lowest absolute value to the largest, covering all the converged spectrum. This procedure is shown in Fig. 5 (a), where the Anderson-Darling test was computed for the 2D Poisson (blue curve) and the GinUE (red curve) distribution, respectively (see Eqs. (16) and (18)). In this figure is clear that the complex spectrum of the Dicke Liouvillian is always well determined by the GinUE distribution along the eigenvalue absolute value with slightly deviations, confirming the chaotic behavior of the spectrum for high coupling strengths.

The last affirmation is corroborated by plotting the spacing distribution of the eigenvalues contained in two selected windows with mean value $|\lambda| = 18.9, 63.5$ in Figs. 5 (b1)-(b2), respectively. In both panels we can see that the eigenvalues contained in each window follow the GinUE distribution (see Eq. (18)), since the Anderson-Darling parameter does not cross the threshold $A^2 = 2.5$. Furthermore, we compute the complex ratio of consecutive eigenvalue spacings for the eigenvalues contained in the same windows (see Eq. (21)), and plot them in Figs. 5 (c1)-(c2). We can see in both panels that the point distribution is avoided at the origin as expected, and it looks fuzzy for small angles. The same panels show the numerical expectation values $\langle r_k \rangle$ and $-\langle \cos(\theta_k) \rangle$ for each set of eigenvalues, which seem to agree with the theoretical expectation values from the GinUE distribution. The deviations are attributed to the low quantity of eigenvalues contained in each window, which must be suppressed when the system size increases; or instead, when the windows are wider containing more eigenvalues.

Now, we present the second case $\gamma = 0.2$, where the isolated classical system shows regular motion [34]. For the real spectrum of the Dicke Hamiltonian with coupling strengths in the normal phase ($\gamma < \gamma_c$), the spectral fluctuations are generally regular (Poisson distribution) [30]. Nevertheless, we follow the same method of studying the complex spectrum of the Dicke Liouvillian taking regions organized by the increasing eigenvalue absolute value (see Fig. 2 (a)).

We take the same moving windows of 500 consecutive eigenvalues and apply the same procedure described above for the case $\gamma = 1$. In Fig. 5 (d) we show the Anderson-Darling test, where we see a more interesting behavior as in the previous case. For the low coupling case we see that the complex spectrum of the Dicke Liouvillian behaves regular following the 2D Poisson distribution at low eigenvalue absolute values, confirming the regular behavior of the spectrum. However, there is a transition region where this integrability breaks around a value $|\lambda| \sim 30$. After this value, there are some fluctuations until the chaotic behavior of the spectrum seems to be reached for values $|\lambda| > 60$. The last finding is im-

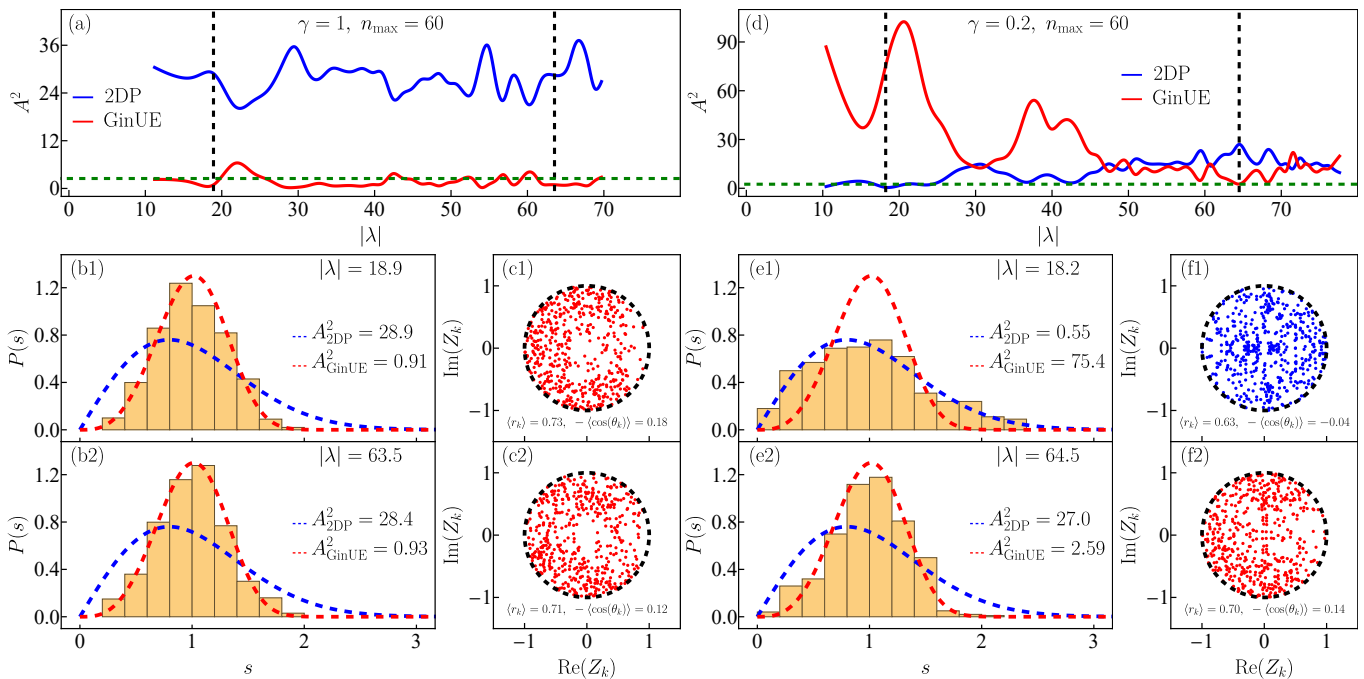


FIG. 5. Panel (a): Anderson-Darling test for the complex spectrum with positive parity of the Dicke Liouvillian and the coupling strength $\gamma = 1$ ($N_{\text{CES}} = 9165$), which was computed numerically for the truncation value $n_{\text{max}} = 60$. The test was computed taking moving windows of the eigenvalue absolute value $|\lambda_k|$ (500 consecutive eigenvalues). The blue (red) curve represents the Anderson-Darling parameter computed for the 2D Poisson (GinUE) distribution (see Eq. (20)). The black dashed vertical lines represent the mean value of the eigenvalue absolute value of selected eigenvalue windows. The green dashed horizontal line represents the Anderson-Darling threshold, $A^2 = 2.5$. Panels (b1)-(b2): Spacing distribution (vanilla bars) for the eigenvalues contained in the windows selected in panel (a), identified with black dashed horizontal lines. The blue (red) dashed curve represents the 2D Poisson (GinUE) distribution (see Eqs. (16) and (18)). Panels (c1)-(c2): Complex ratio of consecutive eigenvalue spacings (red dots, see Eq. (21)) for the eigenvalues contained in the same windows selected in panel (a). Panels (d), (e1)-(e2), and (f1)-(f2): The same as their corresponding panels (a), (b1)-(b2), and (c1)-(c2), for the coupling strength $\gamma = 0.2$ ($N_{\text{CES}} = 11030$). The Liouvillian parameters in all panels are $\omega = \omega_0 = j = \kappa = 1$ and the tolerance value was chosen as $\Delta = 10^{-3}$.

portant, since it suggests that the low coupling strength in the system does not guarantee the regularity of the system for the full complex spectrum.

As in the previous case, we plot the spacing distribution of the eigenvalues contained in two selected windows with mean value $|\lambda| = 18.2, 64.5$ in Figs. 5 (e1)-(e2), respectively. Here, we can see that the eigenvalues contained in the first window follow the 2D Poisson distribution, while the second one seems to follow the GinUE distribution (see Eqs. (16) and (18)). For the first window, the Anderson-Darling parameter does not cross the threshold $A^2 = 2.5$, while for the second window it is in the limit. Moreover, we plot in Figs. 5 (f1)-(f2) the complex ratio of consecutive eigenvalue spacings for the eigenvalues contained in the corresponding windows. We can see in panel (f1) that the point distribution is delocalized over the complex plane as expected, while in panel (f2) the point distribution seems to be avoided at small angles, not at all at the origin. We compute for both cases, the numerical expectation values $\langle r_k \rangle$ and $-\langle \cos(\theta_k) \rangle$ for each set of eigenvalues. The first case seems to agree with the theoretical expectation values

from the 2D Poisson distribution, while the second one with the GinUE distribution. The same deviations are attributed to the low quantity of eigenvalues contained in each window.

Now, we remake the previous analysis increasing the system size and corroborate our statements. We take the system size $j = 3$ ($\mathcal{N} = 6$ atoms) with the same truncation value $n_{\text{max}} = 60$, obtaining $N_{\text{CES}} = 36989, 59001$ converged eigenstates (eigenvalues) for the coupling strengths $\gamma = 0.2, 1$, with a tolerance value $\Delta = 10^{-3}$.

In Fig. 6 we show the results, first for the coupling strength $\gamma = 1$ and then for $\gamma = 0.2$. To perform the Anderson-Darling test, we take moving windows of 1500 consecutive eigenvalues. For the case $\gamma = 1$, we can see in Fig. 6 (a) that the chaotic behaviour of the complex spectrum of the Dicke Liouvillian is again confirmed, where the deviations of the Anderson-Darling parameter computed for the GinUE distribution decrease, showing an almost constant curve. Furthermore, in Figs. 6 (b1)-(b2) we plot the spacing distribution of the eigenvalues contained in two selected windows with mean value

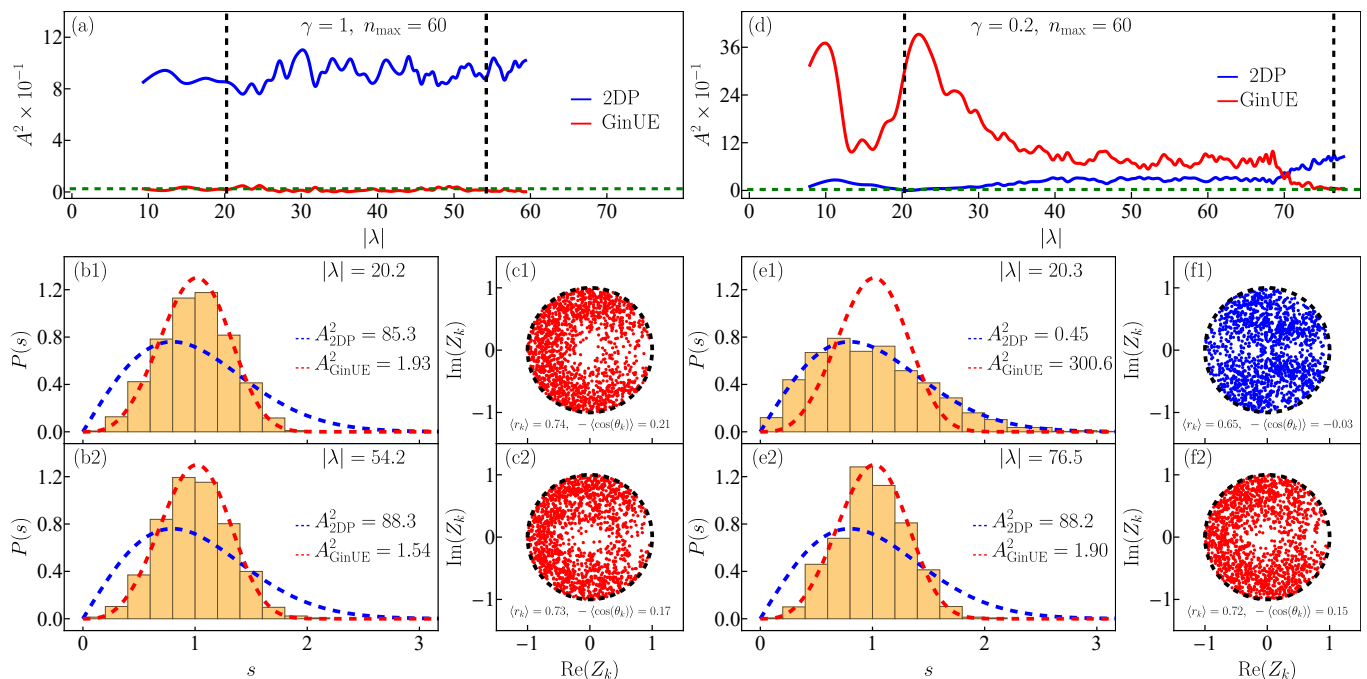


FIG. 6. The same as Fig. 5 for the system size $j = 3$ ($\mathcal{N} = 6$ atoms). For this system size and the truncation value $n_{\max} = 60$ were obtained $N_{\text{CES}} = 36989, 59001$ converged eigenstates (eigenvalues) for the coupling strengths $\gamma = 1, 0.2$ and the moving windows contain 1500 consecutive eigenvalues.

$|\lambda| = 20.2, 54.2$, respectively. We see that not only the spacing distributions follow the GinUE distribution, but also the ratio of consecutive eigenvalue spacings, plotted in Figs. 6 (c1)-(c2) for both windows, shows clearer the avoided regions at the origin and at small angles as expected. In the same way, we see that the agreement of the numerical expectation values $\langle r_k \rangle$ and $-\langle \cos(\theta_k) \rangle$ with the theoretical ones improves as we have argued.

Taking the same moving windows of 1500 consecutive eigenvalues for the case $\gamma = 0.2$, we can see in Fig. 6 (d) the Anderson-Darling test, which confirms the regular behavior of the complex spectrum of the Dicke Liouvillian at low eigenvalue absolute values. Furthermore the transition to chaos is confirmed at high eigenvalue absolute values. This is an interesting feature of the open system, since the transition to chaos is developed slowly until the system behaves chaotic.

For the eigenvalues contained in two selected windows with mean value $|\lambda| = 20.3, 76.5$, we plot in Figs. 6 (e1)-(e2) the spacing distribution. The first window follows the 2D Poisson distribution, while the second one follows the GinUE distribution, confirmed by the Anderson-Darling parameter. Moreover, the ratio of consecutive eigenvalue spacings for both windows is plotted in Figs. 6 (f1)-(f2), showing the complete delocalization of the point distribution in the complex plane for the first window and the avoided regions at the origin and at small angles for the second one. As a matter of fact, we also see a better agreement of the numerical expectation values $\langle r_k \rangle$ and $-\langle \cos(\theta_k) \rangle$ with the theoretical ones.

VI. CONCLUSIONS

We have implemented a convergence criterion for the eigenstates and eigenvalues of the Dicke Liouvillian based in the eigenstate wave functions spread over the Liouville basis. We see that this method seems to be a reasonable proposal, since the number of converged solutions increases with the truncation value of the Liouville space dimension and the statistical behavior of the well-converged eigenvalues remains the same for each truncation value of the Liouville space. Moreover, the last criterion avoids the ambiguity when a convergence criterion based in the change of eigenvalues is implemented, since the complex spectrum of the Dicke Liouvillian seems to be continuous, and the increment of the Liouville space dimension leads to the appearance of new eigenvalues not contained in lower dimensions.

The onset of chaos in the open Dicke model was successfully characterized by applying the standard spectral analysis proposed for dissipative quantum systems. For the high coupling strength case ($\gamma = 1$), we detected the GinUE distribution for the eigenvalue spacings, typical for chaotic open quantum systems for all range of the eigenvalue absolute value of the complex spectrum. On the other hand, for the low coupling strength case ($\gamma = 0.2$), we identified a richer structure of the complex spectrum, since at low eigenvalue absolute values we detect the 2D Poisson distribution for the eigenvalue spacings, typical for regular open quantum systems. Nevertheless, there is a regime where this integrability is bro-

ken and the onset of chaos arises in the system, implying that low coupling strengths do not guarantee the regularity of the system for all the spectrum.

In general, we verify the GHS conjecture to be valid in the open Dicke model, confirming its universality, when the spectral analysis of the Dicke Liouvillian is done by regions of its eigenvalues. We think that these studies are a first step to characterize completely the phenomenon of chaos in the open Dicke model. Further investigations adding other kinds of dissipative channels, as collective atomic decay or temperature effects, are proposed as future work. We think also, that the methods developed in this work can be extended to other open quantum systems with infinite Liouville space.

ACKNOWLEDGMENTS

We thank Jorge G. Hirsch for the reading of this work and his valuable comments and suggestions. We acknowledge the support of the Computation Center - IIMAS, in particular to Adrián Chavesti. In the same way we acknowledge the support of the Computation Center - ICN, in particular to Enrique Palacios, Luciano Díaz, and Eduardo Murrieta. This work was supported by DGAPA-PAPIIT-UNAM under grant No. IG101421 from Mexico. D.V. acknowledges financial support from the postdoctoral fellowship program DGAPA-UNAM.

Appendix A: DIAGONALIZATION OF THE DICKE LIOUVILLIAN

The way to diagonalize a Liouvillian is using the tetradic notation [90], where a matrix representation of the system can be obtained using an arbitrary basis of the form

$$|k, l\rangle\rangle = |k\rangle\langle l|, \quad (\text{A1})$$

where $|\bullet\rangle\rangle$ denotes a vector in the Liouville space composed by all the projectors of the Hilbert-space states $|\bullet\rangle$. For an N -dimensional basis of the Hilbert space, there will be an N^2 -dimensional basis of the Liouville space.

Using the last procedure, the matrix representation of the Dicke Liouvillian takes the form

$$\begin{aligned} L_{k'l',kl}^D &= \langle\langle k', l' | \hat{\mathcal{L}}_D | k, l \rangle\rangle = \text{Tr}\{|l'\rangle\langle k' | \hat{\mathcal{L}}_D | k\rangle\langle l|\} \quad (\text{A2}) \\ &= \sum_i \langle i | l' \rangle \langle k' | \hat{\mathcal{L}}_D | k \rangle \langle l | i \rangle = L_{k'l',kl}^{D,\gamma} + L_{k'l',kl}^{D,\kappa}, \end{aligned}$$

where

$$\begin{aligned} L_{k'l',kl}^{D,\gamma} &= -i \langle\langle k', l' | [\hat{H}_D, \hat{\rho}] | k, l \rangle\rangle \quad (\text{A3}) \\ &= -i (\langle k' | \hat{H}_D | k \rangle \delta_{l,l'} - \langle l | \hat{H}_D | l' \rangle \delta_{k',k}), \end{aligned}$$

and

$$\begin{aligned} L_{k'l',kl}^{D,\kappa} &= \kappa \langle\langle k', l' | (2\hat{a}\hat{\rho}\hat{a}^\dagger - \{\hat{a}^\dagger\hat{a}, \hat{\rho}\}) | k, l \rangle\rangle \quad (\text{A4}) \\ &= 2\kappa \langle k' | \hat{a} | k \rangle \langle l | \hat{a}^\dagger | l' \rangle + \\ &\quad - \kappa (\langle k' | \hat{a}^\dagger \hat{a} | k \rangle \delta_{l,l'} + \langle l | \hat{a}^\dagger \hat{a} | l' \rangle \delta_{k',k}). \end{aligned}$$

1. Fock Basis and Liouville Basis

The standard way to diagonalize the Dicke Hamiltonian is using the Fock basis composed by Dicke states $|j, m_z\rangle$ (with $m_z = -j, -j+1, \dots, j-1, j$) and Fock states $|n\rangle$ (with $n = 0, 1, \dots, \infty$) in tensor product

$$|f\rangle = |n; j, m_z\rangle = |n\rangle \otimes |j, m_z\rangle, \quad (\text{A5})$$

where the index $f(n, m_z) = (2j+1)n + m_z + j + 1$ reorders the elements of the basis with one value. As was mentioned previously, the Fock basis is infinite; nevertheless a truncation finite value n_{\max} for the bosonic subspace is selected in order to solve the system numerically.

The Fock basis can be used to generate the diagonalization basis of the Dicke Liouvillian or Liouville basis

$$|f', f\rangle\rangle = |f'\rangle\langle f| = |n'; j, m'_z\rangle\langle n; j, m_z|, \quad (\text{A6})$$

where the matrix elements of the Dicke Liouvillian are given by

$$\begin{aligned} \langle f' | \hat{H}_D | f \rangle &= (\omega n + \omega_0 m_z) \delta_{n',n} \delta_{m'_z, m_z} + \quad (\text{A7}) \\ &\quad \frac{\gamma}{\sqrt{\mathcal{N}}} (\sqrt{n+1} \delta_{n',n+1} + \sqrt{n} \delta_{n',n-1}) \times \\ &\quad \times (C_{m'_z, m_z}^+ \delta_{m'_z, m_z+1} + C_{m'_z, m_z}^- \delta_{m'_z, m_z-1}) \end{aligned}$$

with $C_{m'_z, m_z}^\pm = \sqrt{j(j+1) - m_z(m_z \pm 1)}$, and

$$\langle f' | \hat{a} | f \rangle = \sqrt{n} \delta_{n',n-1} \delta_{m'_z, m_z}, \quad (\text{A8})$$

$$\langle f' | \hat{a}^\dagger | f \rangle = \sqrt{n+1} \delta_{n',n+1} \delta_{m'_z, m_z}, \quad (\text{A9})$$

$$\langle f' | \hat{a}^\dagger \hat{a} | f \rangle = n \delta_{n',n} \delta_{m'_z, m_z}, \quad (\text{A10})$$

$$\langle f' | \hat{a} \hat{a}^\dagger | f \rangle = (n+1) \delta_{n',n} \delta_{m'_z, m_z}. \quad (\text{A11})$$

2. Dicke Liouvillian with Well-Defined Parity

The Fock basis $|f\rangle$ is an eigenbasis of the parity operator, $\hat{\Pi} = \exp[i\pi(\hat{a}^\dagger \hat{a} + \hat{J}_z + j\hat{1})]$

$$\hat{\Pi} |f\rangle = p |f\rangle, \quad (\text{A12})$$

with eigenvalues $p = (-1)^{(n+m_z+j)} = \pm 1$, and allows to select a basis with well-defined parity in the Hilbert space. The last feature allows in the same way to select a basis with well-defined parity in the Liouville space, when the parity superoperator $\hat{\mathcal{P}}$ acts over the Liouville basis $|f', f\rangle\rangle = |f'\rangle\langle f|$

$$\hat{\mathcal{P}} |f', f\rangle\rangle = \hat{\Pi} |f'\rangle\langle f | \hat{\Pi}^\dagger = P |f', f\rangle\rangle, \quad (\text{A13})$$

with eigenvalues $P = (-1)^{(n'+m'_z-n-m_z)} = \pm 1$.

Appendix B: UNFOLDING OF COMPLEX SPECTRA

The unfolding of complex spectra is needed in order to remove system specific structures from it, in the same way as occurs in the real spectra, and can be implemented in different ways [2, 18, 20, 91]. Following the method presented in Ref. [18], the spectral density of states can be separated in an average (system specific) and a fluctuating (universal) part

$$\nu(\varphi_k) = \sum_{l=1}^N \delta^{(2)}(\varphi_k - \varphi_{k,l}) = \nu_a(\varphi_k) + \nu_f(\varphi_k), \quad (\text{B1})$$

where the averaged spectral density of states is approximated by a sum of Gaussian functions near each complex

eigenvalue $\varphi_k \in \mathbb{C}$ of a set with N elements

$$\nu_a(\varphi_k) \approx \frac{1}{2\pi\sigma^2 N} \sum_{l=1}^N e^{-|\varphi_k - \varphi_{k,l}|^2 / (2\sigma^2)}, \quad (\text{B2})$$

where $\sigma = 4.5S$, $S = N^{-1} \sum_{k=1}^N s_k$, and the spacings $s_k = |\varphi_k - \varphi_k^{1N}|$ are scaled as

$$\tilde{s}_k = \frac{\sqrt{\nu_a(\varphi_k)}}{\tilde{S}} s_k, \quad (\text{B3})$$

with $\tilde{S} = N^{-1} \sum_{k=1}^N \sqrt{\nu_a(\varphi_k)} s_k$.

-
- [1] Edward Ott, *Chaos in Dynamical Systems* (Cambridge University Press, Cambridge, 2002).
- [2] Fritz Haake, *Quantum Signatures of Chaos* (Springer-Verlag, Berlin, 1991).
- [3] T. Guhr, A. Müller-Groeling, and H. A. Weidenmüller, “Random matrix theories in quantum physics: Common concepts,” *Phys. Rep.* **299**, 189 (1998).
- [4] Michael Victor Berry, M. Tabor, and John Michael Ziman, “Level clustering in the regular spectrum,” *Proc. Roy. Soc. London. A. Math. Phys. Sci.* **356**, 375–394 (1977).
- [5] O. Bohigas, M. J. Giannoni, and C. Schmit, “Characterization of chaotic quantum spectra and universality of level fluctuation laws,” *Phys. Rev. Lett.* **52**, 1–4 (1984).
- [6] M. L. Mehta, *Random Matrices* (Academic Press, Boston, 1991).
- [7] Theodore C. Hsu and J. C. Angle’s d’Auriac, “Level repulsion in integrable and almost-integrable quantum spin models,” *Phys. Rev. B* **47**, 14291–14296 (1993).
- [8] V. Zelevinsky, B. A. Brown, N. Frazier, and M. Horoi, “The nuclear shell model as a testing ground for many-body quantum chaos,” *Phys. Rep.* **276**, 85–176 (1996).
- [9] Lea F. Santos and Marcos Rigol, “Onset of quantum chaos in one-dimensional bosonic and fermionic systems and its relation to thermalization,” *Phys. Rev. E* **81**, 036206 (2010).
- [10] H.-P. Breuer and F. Petruccione, *The Theory of Open Quantum Systems* (Oxford University, New York, 2002).
- [11] Howard Carmichael, *An Open Systems Approach to Quantum Optics. Lectures Presented at the Université Libre de Bruxelles, October 28 to November 4, 1991* (Springer-Verlag, Berlin, 1993).
- [12] H. J. Carmichael, *Statistical Methods in Quantum Optics 1: Master Equations and Fokker-Planck Equations* (Springer-Verlag, Berlin, 2002).
- [13] Daniel Manzano, “A short introduction to the Lindblad master equation,” *AIP Advances* **10** (2020), 10.1063/1.5115323, 025106.
- [14] Yuto Ashida, Zongping Gong, and Masahito Ueda, “Non-hermitian physics,” *Adv. Phys.* **69**, 249–435 (2020).
- [15] Rainer Grobe, Fritz Haake, and Hans-Jürgen Sommers, “Quantum distinction of regular and chaotic dissipative motion,” *Phys. Rev. Lett.* **61**, 1899–1902 (1988).
- [16] Jean Ginibre, “Statistical Ensembles of Complex, Quaternion, and Real Matrices,” *J. Math. Phys.* **6**, 440–449 (1965).
- [17] Rainer Grobe and Fritz Haake, “Universality of cubic-level repulsion for dissipative quantum chaos,” *Phys. Rev. Lett.* **62**, 2893–2896 (1989).
- [18] Gernot Akemann, Mario Kieburg, Adam Mielke, and Tomaz Prosen, “Universal signature from integrability to chaos in dissipative open quantum systems,” *Phys. Rev. Lett.* **123**, 254101 (2019).
- [19] Ambuja Bhushan Jaiswal, Akhilesh Pandey, and Ravi Prakash, “Universality classes of quantum chaotic dissipative systems,” *Europhys. Lett.* **127**, 30004 (2019).
- [20] Ryusuke Hamazaki, Kohei Kawabata, Naoto Kura, and Masahito Ueda, “Universality classes of non-Hermitian random matrices,” *Phys. Rev. Res.* **2**, 023286 (2020).
- [21] Álvaro Rubio-García, Rafael A. Molina, and Jorge Dukelsky, “From integrability to chaos in quantum Liouvillians,” *SciPost Phys. Core* **5**, 026 (2022).
- [22] R. H. Dicke, “Coherence in spontaneous radiation processes,” *Phys. Rev.* **93**, 99 (1954).
- [23] Barry M. Garraway, “The Dicke model in quantum optics: Dicke model revisited,” *Philos. Trans. Royal Soc. A* **369**, 1137 (2011).
- [24] Peter Kirton, Mor M. Roses, Jonathan Keeling, and Emanuele G. Dalla Torre, “Introduction to the Dicke model: From equilibrium to nonequilibrium, and vice versa,” *Adv. Quan. Tech.* **2**, 1800043 (2019).
- [25] Clive Emary and Tobias Brandes, “Chaos and the quantum phase transition in the Dicke model,” *Phys. Rev. E* **67**, 066203 (2003).
- [26] Clive Emary and Tobias Brandes, “Quantum chaos triggered by precursors of a quantum phase transition: The Dicke model,” *Phys. Rev. Lett.* **90**, 044101 (2003).
- [27] E. Romera, R. del Real, and M. Calixto, “Husimi distribution and phase-space analysis of a dicke-model quantum phase transition,” *Phys. Rev. A* **85**, 053831 (2012).

- [28] Tobias Brandes, “Excited-state quantum phase transitions in Dicke superradiance models,” *Phys. Rev. E* **88**, 032133 (2013).
- [29] M.A.M de Aguiar, K Furuya, C.H Lewenkopf, and M.C Nemes, “Chaos in a spin-boson system: Classical analysis,” *Ann. Phys.* **216**, 291 – 312 (1992).
- [30] M. A. Bastarrachea-Magnani, S. Lerma-Hernández, and J. G. Hirsch, “Comparative quantum and semiclassical analysis of atom-field systems. II. Chaos and regularity,” *Phys. Rev. A* **89**, 032102 (2014).
- [31] Miguel Angel Bastarrachea-Magnani, Baldemar López del Carpio, Sergio Lerma-Hernández, and Jorge G Hirsch, “Chaos in the Dicke model: quantum and semiclassical analysis,” *Phys. Scr.* **90**, 068015 (2015).
- [32] M. A. Bastarrachea-Magnani, B. López-del Carpio, J. Chávez-Carlos, S. Lerma-Hernández, and J. G. Hirsch, “Delocalization and quantum chaos in atom-field systems,” *Phys. Rev. E* **93**, 022215 (2016).
- [33] M. A. Bastarrachea-Magnani, B. López-del-Carpio, J. Chávez-Carlos, S. Lerma-Hernández, and J. G. Hirsch, “Regularity and chaos in cavity QED,” *Phys. Scr.* **92**, 054003 (2017).
- [34] J. Chávez-Carlos, M. A. Bastarrachea-Magnani, S. Lerma-Hernández, and J. G. Hirsch, “Classical chaos in atom-field systems,” *Phys. Rev. E* **94**, 022209 (2016).
- [35] C. M. Lóbez and A. Relaño, “Entropy, chaos, and excited-state quantum phase transitions in the Dicke model,” *Phys. Rev. E* **94**, 012140 (2016).
- [36] Sudip Sinha and S. Sinha, “Chaos and quantum scars in Bose-Josephson junction coupled to a bosonic mode,” *Phys. Rev. Lett.* **125**, 134101 (2020).
- [37] M. A. M. de Aguiar, K. Furuya, C. H. Lewenkopf, and M. C. Nemes, “Particle-spin coupling in a chaotic system: Localization-delocalization in the Husimi distributions,” *EPL (Europhys. Lett.)* **15**, 125 (1991).
- [38] K Furuya, M.A.M de Aguiar, C.H Lewenkopf, and M.C Nemes, “Husimi distributions of a spin-boson system and the signatures of its classical dynamics,” *Ann. of Phys.* **216**, 313–322 (1992).
- [39] L. Bakemeier, A. Alvermann, and H. Fehske, “Dynamics of the Dicke model close to the classical limit,” *Phys. Rev. A* **88**, 043835 (2013).
- [40] Saúl Pilatowsky-Cameo, David Villaseñor, Miguel A. Bastarrachea-Magnani, Sergio Lerma-Hernández, Lea F. Santos, and Jorge G. Hirsch, “Ubiquitous quantum scarring does not prevent ergodicity,” *Nat. Comm.* **12** (2021), 10.1038/s41467-021-21123-5.
- [41] Saúl Pilatowsky-Cameo, David Villaseñor, Miguel A. Bastarrachea-Magnani, Sergio Lerma-Hernández, Lea F. Santos, and Jorge G. Hirsch, “Quantum scarring in a spin-boson system: fundamental families of periodic orbits,” *New J. Phys.* **23**, 033045 (2021).
- [42] Qian Wang and Marko Robnik, “Statistical properties of the localization measure of chaotic eigenstates in the Dicke model,” *Phys. Rev. E* **102**, 032212 (2020).
- [43] D. Villaseñor, S. Pilatowsky-Cameo, M. A. Bastarrachea-Magnani, S. Lerma-Hernández, and J. G. Hirsch, “Quantum localization measures in phase space,” *Phys. Rev. E* **103**, 052214 (2021).
- [44] Saúl Pilatowsky-Cameo, David Villaseñor, Miguel A. Bastarrachea-Magnani, Sergio Lerma-Hernández, Lea F. Santos, and Jorge G. Hirsch, “Identification of quantum scars via phase-space localization measures,” *Quantum* **6**, 644 (2022).
- [45] Alexander Altland and Fritz Haake, “Equilibration and macroscopic quantum fluctuations in the Dicke model,” *New J. Phys.* **14**, 073011 (2012).
- [46] Michal Kloc, Pavel Stránský, and Pavel Cejnar, “Quantum quench dynamics in Dicke superradiance models,” *Phys. Rev. A* **98**, 013836 (2018).
- [47] Sergio Lerma-Hernández, Jorge Chávez-Carlos, Miguel A. Bastarrachea-Magnani, Lea F. Santos, and Jorge G. Hirsch, “Analytical description of the survival probability of coherent states in regular regimes,” *J. Phys. A* **51**, 475302 (2018).
- [48] S. Lerma-Hernández, D. Villaseñor, M. A. Bastarrachea-Magnani, E. J. Torres-Herrera, L. F. Santos, and J. G. Hirsch, “Dynamical signatures of quantum chaos and relaxation time scales in a spin-boson system,” *Phys. Rev. E* **100**, 012218 (2019).
- [49] David Villaseñor, Saúl Pilatowsky-Cameo, Miguel A Bastarrachea-Magnani, Sergio Lerma, Lea F Santos, and Jorge G Hirsch, “Quantum vs classical dynamics in a spin-boson system: manifestations of spectral correlations and scarring,” *New J. Phys.* **22**, 063036 (2020).
- [50] Jorge Chávez-Carlos, B. López-del Carpio, Miguel A. Bastarrachea-Magnani, Pavel Stránský, Sergio Lerma-Hernández, Lea F. Santos, and Jorge G. Hirsch, “Quantum and classical lyapunov exponents in atom-field interaction systems,” *Phys. Rev. Lett.* **122**, 024101 (2019).
- [51] R. J. Lewis-Swan, A. Safavi-Naini, J. J. Bollinger, and A. M. Rey, “Unifying , thermalization and entanglement through measurement of fidelity out-of-time-order correlators in the Dicke model,” *Nat. Comm.* **10**, 1581 (2019).
- [52] Saúl Pilatowsky-Cameo, Jorge Chávez-Carlos, Miguel A. Bastarrachea-Magnani, Pavel Stránský, Sergio Lerma-Hernández, Lea F. Santos, and Jorge G. Hirsch, “Positive quantum lyapunov exponents in experimental systems with a regular classical limit,” *Phys. Rev. E* **101**, 010202(R) (2020).
- [53] Aleksandrina V Kirkova and Peter A Ivanov, “Quantum chaos and thermalization in the two-mode Dicke model,” *Phys. Scr.* **98**, 045105 (2023).
- [54] K. Furuya, M. C. Nemes, and G. Q. Pellegrino, “Quantum dynamical manifestation of chaotic behavior in the process of entanglement,” *Phys. Rev. Lett.* **80**, 5524–5527 (1998).
- [55] S. Ray, A. Ghosh, and S. Sinha, “Quantum signature of chaos and thermalization in the kicked Dicke model,” *Phys. Rev. E* **94**, 032103 (2016).
- [56] David Villaseñor, Saúl Pilatowsky-Cameo, Miguel A. Bastarrachea-Magnani, Sergio Lerma-Hernández, Lea F. Santos, and Jorge G. Hirsch, “Chaos and thermalization in the spin-boson Dicke model,” *Entropy* **25** (2023), 10.3390/e25010008.
- [57] Tuomas Jaako, Ze-Liang Xiang, Juan José Garcia-Ripoll, and Peter Rabl, “Ultrastrong-coupling phenomena beyond the Dicke model,” *Phys. Rev. A* **94**, 033850 (2016).
- [58] Markus P. Baden, Kyle J. Arnold, Arne L. Grimsmo, Scott Parkins, and Murray D. Barrett, “Realization of the Dicke model using cavity-assisted Raman transitions,” *Phys. Rev. Lett.* **113**, 020408 (2014).
- [59] Zhiqiang Zhang, Chern Hui Lee, Ravi Kumar, K. J. Arnold, Stuart J. Masson, A. L. Grimsmo, A. S. Parkins, and M. D. Barrett, “Dicke-model simulation via cavity-assisted Raman transitions,” *Phys. Rev. A* **97**, 043858 (2018).

- [60] J Cohn, A Safavi-Naini, R J Lewis-Swan, J G Bohnet, M Gärttner, K A Gilmore, J E Jordan, A M Rey, J J Bollinger, and J K Freericks, “Bang-bang shortcut to adiabaticity in the Dicke model as realized in a penning trap experiment,” *New J. Phys.* **20**, 055013 (2018).
- [61] A. Safavi-Naini, R. J. Lewis-Swan, J. G. Bohnet, M. Gärttner, K. A. Gilmore, J. E. Jordan, J. Cohn, J. K. Freericks, A. M. Rey, and J. J. Bollinger, “Verification of a many-ion simulator of the Dicke model through slow quenches across a phase transition,” *Phys. Rev. Lett.* **121**, 040503 (2018).
- [62] F. Dimer, B. Estienne, A. S. Parkins, and H. J. Carmichael, “Proposed realization of the Dicke-model quantum phase transition in an optical cavity QED system,” *Phys. Rev. A* **75**, 013804 (2007).
- [63] Peter Kirton and Jonathan Keeling, “Superradiant and lasing states in driven-dissipative Dicke models,” *New J. Phys.* **20**, 015009 (2018).
- [64] Jan Gelhausen and Michael Buchhold, “Dissipative Dicke model with collective atomic decay: Bistability, noise-driven activation, and the nonthermal first-order superradiance transition,” *Phys. Rev. A* **97**, 023807 (2018).
- [65] Federico Carollo and Igor Lesanovsky, “Exactness of mean-field equations for open Dicke models with an application to pattern retrieval dynamics,” *Phys. Rev. Lett.* **126**, 230601 (2021).
- [66] Mario Boneberg, Igor Lesanovsky, and Federico Carollo, “Quantum fluctuations and correlations in open quantum Dicke models,” *Phys. Rev. A* **106**, 012212 (2022).
- [67] Simon B. Jäger, Tom Schmit, Giovanna Morigi, Murray J. Holland, and Ralf Betzholz, “Lindblad master equations for quantum systems coupled to dissipative bosonic modes,” *Phys. Rev. Lett.* **129**, 063601 (2022).
- [68] Kevin C. Stitely, Andrus Giraldo, Bernd Krauskopf, and Scott Parkins, “Nonlinear semiclassical dynamics of the unbalanced, open Dicke model,” *Phys. Rev. Res.* **2**, 033131 (2020).
- [69] Mahaveer Prasad, Hari Kumar Yadalam, Camille Aron, and Manas Kulkarni, “Dissipative quantum dynamics, phase transitions, and non-hermitian random matrices,” *Phys. Rev. A* **105**, L050201 (2022).
- [70] Sayak Ray, Amichay Vardi, and Doron Cohen, “Quantum signatures in quench from chaos to superradiance,” *Phys. Rev. Lett.* **128**, 130604 (2022).
- [71] Louis Garbe, Peregrine Wade, Fabrizio Minganti, Nathan Shammah, Simone Felicetti, and Franco Nori, “Dissipation-induced bistability in the two-photon Dicke model,” *Sci. Rep.* **10**, 13408 (2020).
- [72] Jiahui Li, Rosario Fazio, and Stefano Chesi, “Nonlinear dynamics of the dissipative anisotropic two-photon Dicke model,” *New J. Phys.* **24**, 083039 (2022).
- [73] Zhang Zhiqiang, Chern Hui Lee, Ravi Kumar, K. J. Arnold, Stuart J. Masson, A. S. Parkins, and M. D. Barrett, “Nonequilibrium phase transition in a spin-1 Dicke model,” *Optica* **4**, 424–429 (2017).
- [74] Jens Klinder, Hans Keßler, Matthias Wolke, Ludwig Mathey, and Andreas Hemmerich, “Dynamical phase transition in the open Dicke model,” *Proc. Nat. Ac. Sci.* **112**, 3290–3295 (2015).
- [75] Klaus Hepp and Elliott H Lieb, “On the superradiant phase transition for molecules in a quantized radiation field: the Dicke maser model,” *Ann. Phys. (N.Y.)* **76**, 360 – 404 (1973).
- [76] Klaus Hepp and Elliott H. Lieb, “Equilibrium statistical mechanics of matter interacting with the quantized radiation field,” *Phys. Rev. A* **8**, 2517–2525 (1973).
- [77] Y. K. Wang and F. T. Hioe, “Phase transition in the Dicke model of superradiance,” *Phys. Rev. A* **7**, 831–836 (1973).
- [78] Mor M. Roses and Emanuele G. Dalla Torre, “Dicke model,” *PLOS ONE* **15**, 1–8 (2020).
- [79] Berislav Buča and Tomaž Prosen, “A note on symmetry reductions of the Lindblad equation: transport in constrained open spin chains,” *New J. Phys.* **14**, 073007 (2012).
- [80] Victor V. Albert and Liang Jiang, “Symmetries and conserved quantities in lindblad master equations,” *Phys. Rev. A* **89**, 022118 (2014).
- [81] Simon Lieu, Ron Belyansky, Jeremy T. Young, Rex Lundgren, Victor V. Albert, and Alexey V. Gorshkov, “Symmetry breaking and error correction in open quantum systems,” *Phys. Rev. Lett.* **125**, 240405 (2020).
- [82] Miguel A Bastarrachea-Magnani and Jorge G Hirsch, “Efficient basis for the Dicke model: I. Theory and convergence in energy,” *Phys. Scr.* **2014**, 014005 (2014).
- [83] Jorge G Hirsch and Miguel A Bastarrachea-Magnani, “Efficient basis for the Dicke model: II. Wave function convergence and excited states,” *Phys. Scr.* **2014**, 014018 (2014).
- [84] W. Kerner, K. Lerbinger, and J. Steuerbald, “Computing complex eigenvalues of large non-Hermitian matrices,” *Comp. Phys. Comm.* **38**, 27–37 (1985).
- [85] M. V. Berry, “Regular and irregular semiclassical wavefunctions,” *J. Phys. A* **10**, 2083–2091 (1977).
- [86] T. W. Anderson and D. A. Darling, “Asymptotic Theory of Certain “Goodness of Fit” Criteria Based on Stochastic Processes,” *Ann. Math. Stat.* **23**, 193 – 212 (1952).
- [87] Vadim Oganesyan and David A. Huse, “Localization of interacting fermions at high temperature,” *Phys. Rev. B* **75**, 155111 (2007).
- [88] Y. Y. Atas, E. Bogomolny, O. Giraud, and G. Roux, “Distribution of the ratio of consecutive level spacings in random matrix ensembles,” *Phys. Rev. Lett.* **110**, 084101 (2013).
- [89] Lucas Sá, Pedro Ribeiro, and Tomaž Prosen, “Complex spacing ratios: A signature of dissipative quantum chaos,” *Phys. Rev. X* **10**, 021019 (2020).
- [90] Shaul Mukamel, *Principles of Nonlinear Optical Spectroscopy* (Oxford University Press, New York, 1995).
- [91] H. Markum, R. Pullirsch, and T. Wettig, “Non-Hermitian random matrix theory and lattice QCD with chemical potential,” *Phys. Rev. Lett.* **83**, 484–487 (1999).